VIRTUAL-PILOT-IN-THE-LOOP SIMULATION MODEL TO ASSESS HELICOPTER ROUTES FEASIBILITY

Francesca Roncolini*, Giuseppe Quaranta
Politecnico di Milano, Dipartimento di Scienze e Tecnologie Aerospaziali, Milano - Italy
* Corresponding author, email:francesca.roncolini@polimi.it

Abstract

A virtual-pilot-in-the-loop reference tracking simulation environment is set up in order to analyze the feasibility of candidate trajectories. The helicopter is modeled as a linear state-space dynamics, and the pilot is modeled by means of the revised optimal control pilot model (ROCM). The pilot's neuromuscular dynamics and processing delay are modeled as second-order dynamics, augmenting the system states from 9 to 25. A guidance logic is implemented to allow the trajectory tracking. The pilot's workload is assessed by means of the computation of the aggression factor, related to the control input rates. The pilot-in-the-loop simulator performs a good trajectory tracking, even if some adjustments need to be introduced in the guidance logic, and is able to detect some level of criticality in the analyzed trajectories.

LIST OF ACRONYMS

u	Helicopter longitudinal speed (body axes)
v	Helicopter lateral speed (body axes)
w	Helicopter vertical speed (body axes)
p	Roll rate
q	Pitch rate
r	Yaw rate
ϕ	Euler-321 roll angle
θ	Euler-321 pitch angle
ψ	Euler-321 heading angle
θ_0	Main rotor collective angle
θ_{1s}	Main rotor longitudinal cyclic angle
θ_{1c}	Main rotor lateral cyclic angle
θ_{0T}	Tail rotor collective angle
X	Longitudinal external force (body axes)
Y	Lateral external force (body axes)
Z	Vertical external force (body axes)
L	External moment about body x axis
M	External moment about body y axis
N	External moment about body z axis
M_a	Helicopter mass
I_{aa}	Moment of inertia about axis a
I_{ab}	Product of inertia of axes a and b
ξ_{nm}	Neuromuscular damping
ω_{nm}	Neuromuscular natural frequency
γ	Ramp angle
χ	Azimuth angle

1. INTRODUCTION

Virtual prototypes and mathematical models are a powerful assessment instrument during several phases of the flying vehicle life-cycle, from the preliminary design to certification, as explained by Padfield [1]. Certain certification flight test activities, particularly those involving hazardous maneuvers, can be classified as high-risk in terms of flight safety, therefore the possibility to involve flight simulations in the certification process is currently widely evaluated [2].
For instance, in this document by Avi et al. [3] is reported a possible methodology to validate and certify Point-in-Space (PinS) helicopter routes with the help of simulation: the route is designed by means of a path planner, then the GNSS signal level and the presence of obstacles on the designed route are checked by means of a UAV. The pilot's workload, dependent on the control effort, and the compliance with the helicopter performance constraints, represented by limitations on the attitude, rates and load factor, are assessed by means of closed-loop simulations where both the dynamics of the pilot and of the rotorcraft are modeled, as indicated in Fig. 1.
The simulations would avoid:

1. the costs involved in a flight campaign aimed at collecting the necessary data. Considering that there may be several iterations before finding a

route compatible with the pilot's workload and the helicopter performance constraints, there would be multiple flights required;

2. the risks of performing this experimental activity without checking the range of workload and performance implied by the route beforehand.

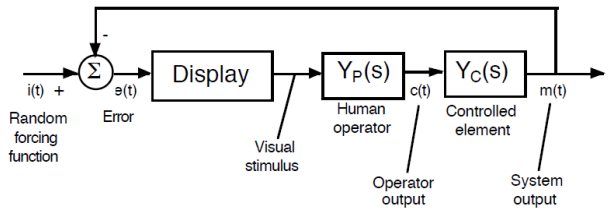

Figure 1: Closed pilot-in-the-loop simulation model

This paper is the continuation of the work described in [4], where, similarly to [3] , the manned-unmanned teaming (MUM-T) configuration is exploited in order to design safe routes. In this case, the MUM-T solution is addressed to arduous HEMS operations in mountainous and unknown areas: a reference route is designed by means of a path planning algorithm basing on the available maps of the area, and the route is continuously updated according to the possible obstacles detected by the UAV.

In order to check the real feasibility of a designed route, some quantities such as the pilot's control effort, the helicopter attitude and rates and the load factor can be analyzed. To obtain this quantities, it is necessary to perform a reference tracking closed-loop simulation that features both the helicopter and the pilot dynamics.

The objective of the present paper is to provide and describe a possible methodology to set up such a reference tracking simulation, with a particular focus on the choice and design of the pilot model.

The proposed methodology can be used in any reference tracking vehicle simulation, because it is not strictly related to the MUM-T application described above, and the vehicle types (rotorcraft / aircraft / automobiles) are interchangeable.

2. METHODS AND MODELS

2.1. Helicopter model

The helicopter nonlinear equations of motion are represented by the compact form described by Eq. 1:

$$\dot{\mathbf{x}} = \mathbf{F}(\mathbf{x}, \mathbf{u}, t) \tag{1}$$

where the motion states are

$$\mathbf{x} = \{u, w, q, \theta, v, p, \phi, r, \psi\} \tag{2}$$

and the control vector is

$$\mathbf{u} = \{\theta_0, \theta_{1s}, \theta_{1c}, \theta_{0T}\} \tag{3}$$

The expanded form of Eq. 1 is:

$$\begin{aligned}
\dot{u} &= -(wq - vr) + \frac{X}{M_a} - g sin\theta \\
\dot{v} &= -(ur - wp) + \frac{Y}{M_a} + g cos\theta sin\phi \\
\dot{w} &= -(vp - uq) + \frac{Z}{M_a} + g cos\theta cos\phi \\
I_{xx}\dot{p} &= (I_{yy} - I_{zz})qr + I_{xz}(\dot{r} + pq) + L \\
I_{yy}\dot{q} &= (I_{zz} - I_{xx})rp + I_{xz}(r^2 + p^2) + M \\
I_{zz}\dot{r} &= (I_{xx} - I_{yy})pq + I_{xz}(\dot{p} + qr) + N \\
\dot{\phi} &= p + q\, sin\phi\, tan\theta + r\, cos\phi\, tan\theta \\
\dot{\theta} &= q\, cos\phi - r\, sin\phi \\
\dot{\psi} &= q\, sin\phi\, sec\theta + r\, cos\phi\, sec\theta
\end{aligned} \tag{4}$$

Supposing that the forces X, Y, Z and the moments L, M, N are themselves function of the control input, and of the motion variables and their derivatives, the above equations can be linearized about a trim point, as extensively explained in the fourth chapter of [5], to obtain a state-space form of the type:

$$\begin{aligned}
\dot{\mathbf{x}} &= \mathbf{Ax} + \mathbf{Bu} \\
\mathbf{y} &= \mathbf{Cx} + \mathbf{Du}
\end{aligned} \tag{5}$$

The helicopter models used to set up and test the closed-loop simulation environment are state-space models obtained by the linearization of three different helicopters dynamics about the trim point of straight level flight at the airspeed of $30\ m/s$. The three helicopters are: the twin engine 4.5-ton category Westland Lynx; the twin engine 2.5-ton category Eurocopter Bo105; the twin engine 6-ton category SA Puma.

The state-space models of these helicopters are taken from Appendix 4B of [5], which contains the state-space dynamics representation of the three helicopters at different airspeeds.

The A and B matrices for Lynx, Puma and Bo105 at 30 m/s straight level flight are reported in Appendix A.

2.2. Pilot model

The pilot can be seen as either a passive element, who acts as a bio-dynamic feedthrough, or an active element, who exerts a voluntary control action on the vehicle by means of the control inputs. In this study, the pilot is intended as an active element.
As reported in [6], there are two major fashions in the science of human pilot modeling: the frequency-based modeling and the time-based modeling.
The frequency-based models rely on classical control techniques, and include renowned models such as the crossover model, the precision model, the extensively used Tustin-McRuer model, and the structural model. The time-based models rely on modern control techniques and include the optimal control model and its variations.
The major difference between the two fashions is that the frequency-based models are more suited to single axis control, with the exception of the simplified structural model presented in [7], which however does not allow inter-axis coupling, while the time-based models rely on full state feedback optimal control techniques which depend on state-space models that can describe MIMO systems with interaxis coupling.
Given the above reasons, and considered that the application in question regards helicopters, which are MIMO systems subject to interaxis coupling, it has been decided to choose a time-based model.

The revised optimal control model This model, described in [8], is a variation of the more famous optimal control model [9]. The fundamental assumption behind these models is that the pilot behaves as an optimal controller, therefore choosing their gains in order to minimize a quadratic cost function of the form:

(6)
$$J(\mathbf{u}) = \lim_{T\to\infty} E\left(\frac{1}{T}\int_0^T ((\mathbf{r}-\mathbf{x})^T\mathbf{Q}(\mathbf{r}-\mathbf{x}) + \mathbf{u}^T\mathbf{R}\mathbf{u})\,dt\right)$$

where r is the reference state that has to be tracked, Q is a positive semi-definite matrix and R is positive definite. By solving the associated Riccati equation (for example using the lqr function in Matlab) it is possible to find the gain matrix K that will multiply the states in the full state feedback: $\mathbf{u} = \mathbf{K}(\mathbf{r}-\mathbf{x})$.
However, the pilot is not really a simple optimal controller. Indeed, as is depicted in Fig. 2, the pilot observes an output that is usually only a part of the state vector subject to an observation noise and to a visual delay.

Then, the pilot estimates the full state from the noisy output and the estimation process can be modeled as a Kalman filter. For the sake of simplicity, in the model discussed in this paper the Kalman filtering has been neglected, and the estimated state has been identified with the helicopter model output.
At this point, the pilot needs an amount of time, called the central processing delay, to process the information and compute a control action, which is transferred from the brain to the limb by means of the neuromuscular dynamics.

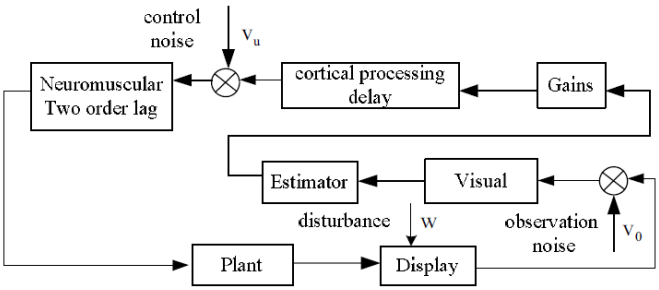

Figure 2: Revised optimal control pilot model

The neuromuscular dynamics is described by the transfer function:

(7)
$$G_{nm} = \frac{\omega_{nm}^2}{s^2 + 2\xi_{nm}\omega_{nm}s + \omega_{nm}^2}$$

where ξ_{nm} can be set to 0.707 and ω_{nm} can be set to 10 rad/s. The reasons for this choice of parameters is based upon electromyogram measurements reported in [10].
The visual and central processing time delays (average values: 0.075 and 0.03 seconds) are gathered in a unique time delay, called the processing delay, which includes also the nerve conduction time (average value: 0.03 seconds). The processing delay can be therefore considered to have a value of 0.14 seconds, and is modeled by means of the second-order Padé approximation:

(8)
$$G_d = \frac{s^2 - \frac{6}{\tau_p}s + \frac{12}{\tau_p^2}}{s^2 + \frac{6}{\tau_p}s + \frac{12}{\tau_p^2}}$$

Each output of the control law is fed through the processing delay and neuromuscular dynamics, as shown in Fig. 3.

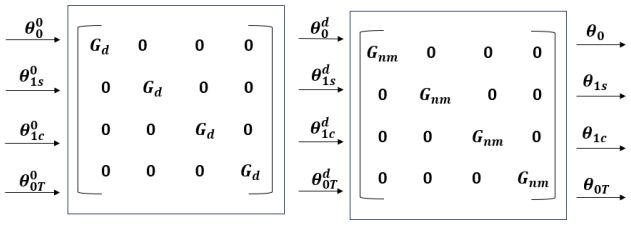

Figure 3: Delay and neuromuscular dynamics

Therefore for each control input four states, two from the processing delay dynamics and two from the neuromuscular dynamics, are added to the original helicopter state-space dynamics. The system, which had initially 9 states, has now 25 states.
The MIMO system from u_0 to u_d has 8 states and can be written as the state-space 9:

$$\begin{aligned} \dot{x}_d &= A_d x_d + B_d u_0 \\ u_d &= C_d x_d + D_d u_0 \end{aligned} \tag{9}$$

Also the MIMO system from u_d to u has 8 states, and can be represented by the state-space 10:

$$\begin{aligned} \dot{x}_{nm} &= A_{nm} x_{nm} + B_{nm} u_d \\ u &= C_{nm} x_{nm} \end{aligned} \tag{10}$$

The complete augmented state-space from u_0 to y will have the form:

$$\begin{aligned} \begin{bmatrix} \dot{x} \\ \dot{x}_{nm} \\ \dot{x}_d \end{bmatrix} &= \begin{bmatrix} A & BC_{nm} & 0 \\ 0 & A_{nm} & B_{nm}C_d \\ 0 & 0 & A_d \end{bmatrix} \begin{bmatrix} x \\ x_{nm} \\ x_d \end{bmatrix} + \begin{bmatrix} 0 \\ B_{nm}D_d \\ B_d \end{bmatrix} u_0 \\ y &= \begin{bmatrix} I & 0 & 0 \\ 0 & 0 & 0 \\ 0 & 0 & 0 \end{bmatrix} \begin{bmatrix} x \\ x_{nm} \\ x_d \end{bmatrix} \end{aligned} \tag{11}$$

The optimal control law is applied to the augmented system, therefore the cost function to be minimized will be:

$$J(u_0) = \lim_{T\to\infty} E\left(\frac{1}{T}\int_0^T ((r^* - \eta)^T Q^* (r^* - \eta) + u_0^T R u_0)\, dt\right) \tag{12}$$

where $r^* = [r \;\; 0 \;\; 0]$, η is the augmented state, and $Q^* = \begin{bmatrix} Q & 0 & 0 \\ 0 & 0 & 0 \\ 0 & 0 & 0 \end{bmatrix}$.
The Q and R matrices gains were tuned by trials until good reference tracking performance were achieved. The matrices used in the simulations are:

$$\begin{aligned} Q &= diag\{100, 100, 1, 1, 100, 1, 1, 1, 100\} \\ R &= diag\{100, 100, 100, 100\} \end{aligned} \tag{13}$$

The gains of the Q matrix were set to 100 for the controlled states, and 1 for the other states.

2.3. Guidance logic

The guidance logic is the logic followed to generate the reference states as the helicopter flies the route.
The route is composed by waypoints, defined by positions in the East - North - Up reference frame. However, the helicopter state vector does not contain the position, but the velocity in the body reference frame.
Therefore, the reference states used to control the helicopter are the velocities in the body reference frame u, v, w, and the heading angle ψ, and they are defined as follows:

$$\begin{aligned} \begin{bmatrix} u_{ref} \\ v_{ref} \\ w_{ref} \end{bmatrix} &= R_{MAP->BODY} \begin{bmatrix} V_\infty \cos\gamma \sin\chi \\ V_\infty \cos\gamma \cos\chi \\ V_\infty \sin\gamma \end{bmatrix} \\ \psi_{ref} &= \chi \end{aligned} \tag{14}$$

where V_∞ is the reference airspeed, constant along the route, $R_{MAP->BODY}$ is the rotation matrix from the map reference frame to the body frame, and γ and χ are the ramp angle and the azimuth angle of the route in the current position of the helicopter.
γ and χ are updated as illustrated in Fig. 4: when the helicopter enters in a region within a certain radius from the reference waypoint, γ and χ shift to the ones corresponding to the following portion.
With this strategy, it is possible to follow the path by using velocity reference instead of position reference. However, at each waypoint there will be a loss of precision, therefore the longer is the route, the less precise will be the final position.
Another problem of this guidance logic is that the reference states are non-smooth signals: in particular the discontinuities in the heading angle will cause yaw and pitch rate to achieve very high peaks, which shall be filtered.

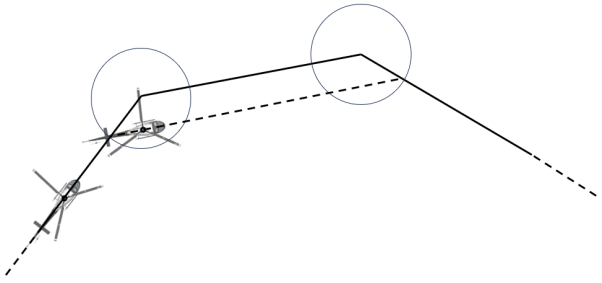

Figure 4: Guidance logic

2.4. Workload assessment

The workload of the pilot has been assessed by means of the control input rates.
According to [11], there is a relationship between the control input rate and the Bedford scale rating for the subjective workload, illustrated in Fig. 5: the aggression factor, which depends on the input rate, is proportional to the Bedford rating by a Pearson correlation coefficient, which is different for each control axis.
The aggression factor is defined as:

$$A(\delta) = \frac{1}{T}\int_{t}^{t+T} |\dot{\delta}|\, dt \tag{15}$$

where δ is the control input travel in [mm], and T is the time window length. A gain of $5/3$ has been used to convert the control inputs from [°] to [mm], and a window length of 6 seconds was used. The window length depends on the average duration of the specific maneuvers that compose the flight.
The control input derivatives are filtered by means of a first-order low-pass filter with a time constant of 0.1 s to avoid the peaks caused by discontinuities in the reference states.

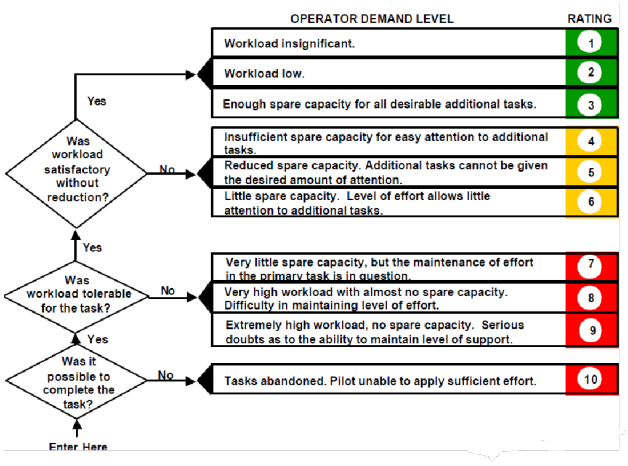

Figure 5: Bedford scale

The correlation coefficients that relate the aggression factor to the Bedford rating are reported in Tab. 1

Collective	Longitudinal	Lateral
$c = 0.63$	$c = 0.72$	$c = 0.67$

Table 1: Pearson correlation coefficients - Aggression factor vs. Bedford

3. TESTS AND RESULTS

3.1. Objective of the tests

The tests aim at using the pilot-in-the-loop simulation environment to check if the planned trajectory is feasible in terms of the helicopter dynamics and pilot's workload.
The trajectories planning is performed by means of the path planner described in [4]. This planner uses the Rapidly-exploring Random Tree algorithm and its improved versions combined with the Dubins curves path design strategy in order to plan a path from a starting point to the end point respecting some performance constraints, that are:

- maximum roll angle, set to $60°$;
- flight path angle limits, set to $\pm 25°$;
- airspeed, set to 30 m/s.

These performance constraints don't have to be intended as dynamic constraints, but as kinematic constraints: the path is not constrained to the dynamics of the specific helicopter to limit its output, instead it is bound to the assumption that the constraints on the maximum roll angle, flight path angle and airspeed are respected in each point of the trajectory. The relationship between the assumptions on the performance constraints and the trajectory planning is illustrated in [12].
As a consequence, it is not guaranteed that the roll angle of the helicopter remains lower than $60°$ during the whole trajectory, or that the airspeed remains equal to 30 m/s: it must be verified.
In conclusion, the signals that will be analyzed to establish if the trajectory is feasible are:

1. The attitude, with a particular attention on the roll angle, comparing it with the limitation of $60°$;
2. The airspeed, comparing it to the reference airspeed of 30 m/s;
3. The trajectory followed by the pilot, comparing it to the reference trajectory;
4. The pilot workload during the flight, compared to the acceptable values of the Bedford scale.

The results presented in this paper concern two trajectories planned in La Maddalena island, in Northern Sardinia, Italy. The trajectories are:

1. The reference trajectory, planned by means of the quasi-optimal RRT* algorithm basing on the database terrain elevation data;

2. The trajectory replanned after the "reconnaissance" UAV detects an obstacle on the reference route (could be bad weather, turbulence, power cables...). The replanned route is planned by cutting the reference route some states before the obstacles and using a fast but non-optimal algorithm such as the bidirectional RRT to create a new path from the truncated state to the end point.

Both the trajectories are smoothed by means of a Savitzky-Golay filter. The two routes are shown in Fig. 6.

3.2. Results

The results presented here are relative to the Puma helicopter. The results for the Lynx and Bo105 are shown in Appendix B.
The simulations have been carried out with the software Matlab/Simulink R2021b.

3.2.1. Reference route

Fig 7 shows that the reference trajectory can be followed by the helicopter, with a loss of precision towards the end as explained in the guidance logic section.

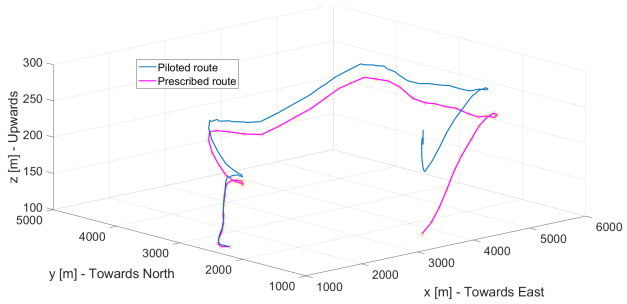

Figure 7: Prescribed vs. followed reference route

Fig. 8 shows that the roll angle lies within the prescribed limits, and Fig. 9 illustrates how the airspeed correctly tracks the reference airspeed.

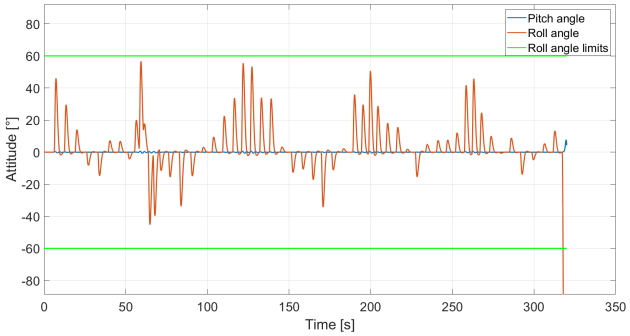

Figure 8: Attitude vs. attitude limits, reference route

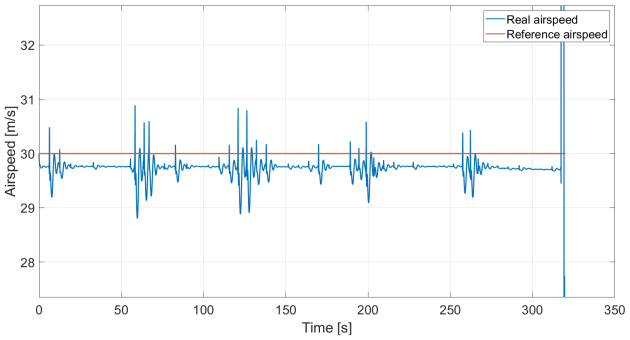

Figure 9: Airspeed vs. reference airspeed, reference route

The workload, represented in Fig. 10, is totally acceptable for what concerns the collective and longitudinal axes, and it is apparently not tolerable in at least three portions of the trajectory for what concerns the lateral axis, referring to the Bedford scale presented in Fig. 5. Whether it is a numerical problem due to the discontinuity of the reference heading angle or it reflects the reality has to be further investigated.

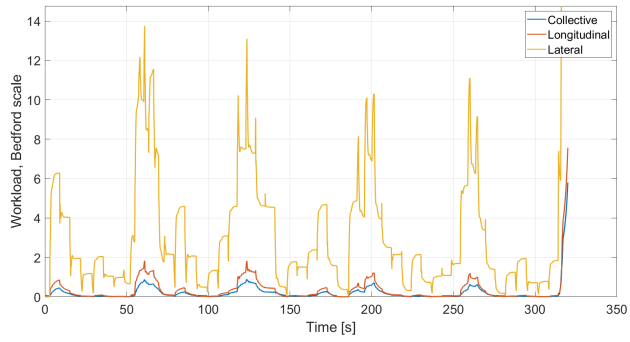

Figure 10: Workload, reference route

3.2.2. Replanned route

The tracking of the replanned trajectory appears to be generally good, apart from a problematic point, indicated between red lines in Figs. 11, 12, 13, 14, where

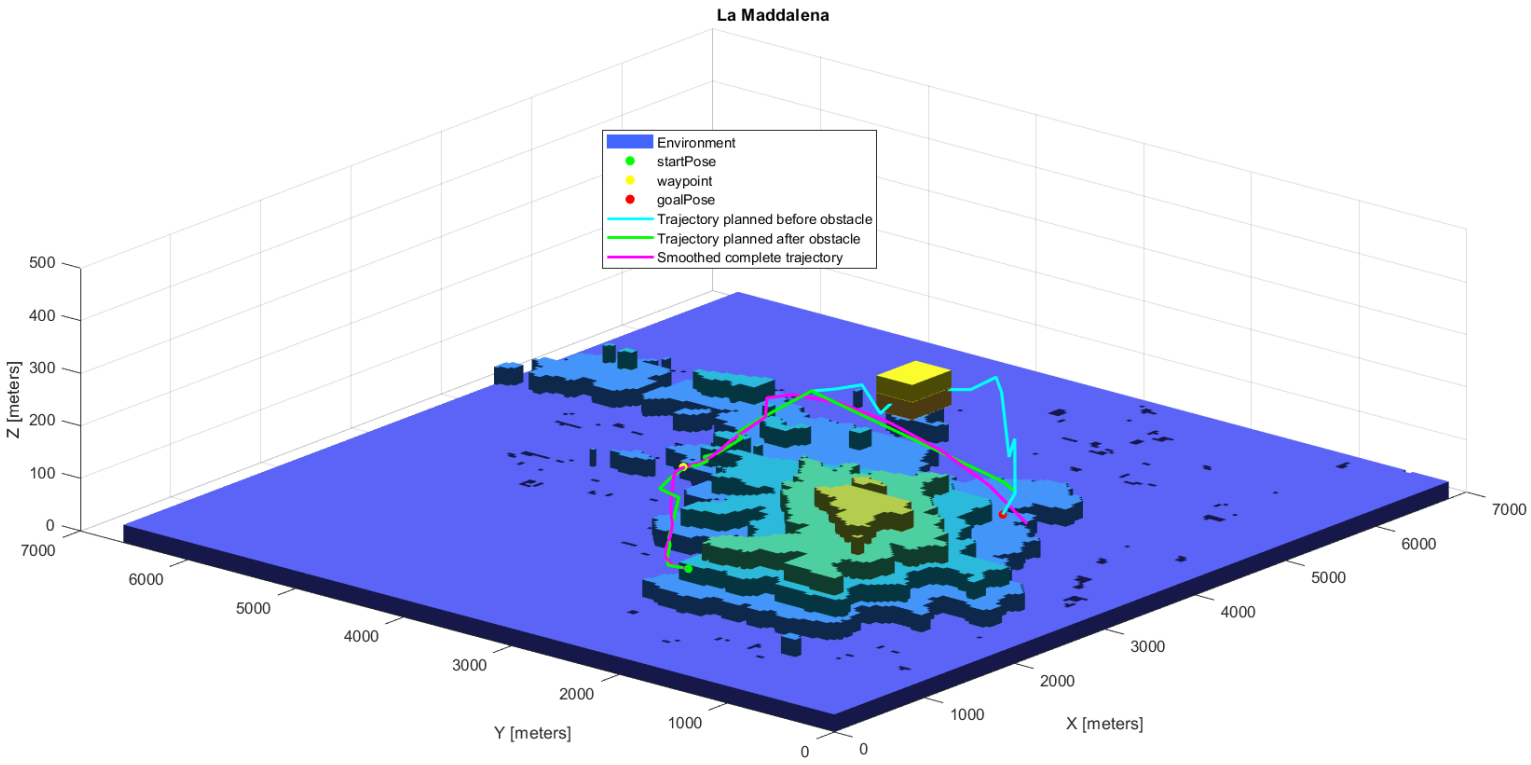

Figure 6: Reference and replanned trajectories

the roll angle and the workload are totally unacceptable.

Observing Fig. 6 it is possible to see that the problematic portion of the route is present only in the replanned trajectory after the smoothing has been carried out, and not in the original replanned trajectory: therefore, the problem may lie in the Savitzky-Golay smoothing filter.

This point will be further investigated in the future, and the pilot-in-the-loop simulator can be used to assess the Savitzky-Golay filtering performance, and to set the filter type and options.

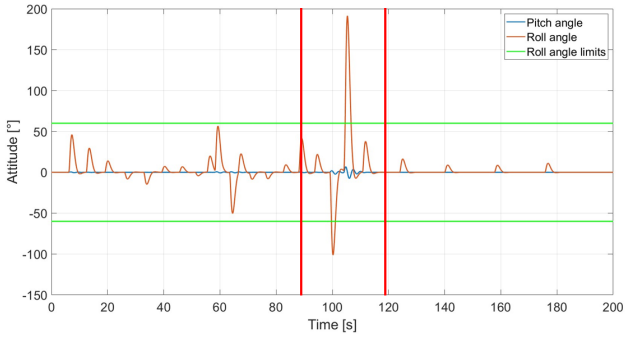

Figure 12: Attitude vs. attitude limits, replanned route

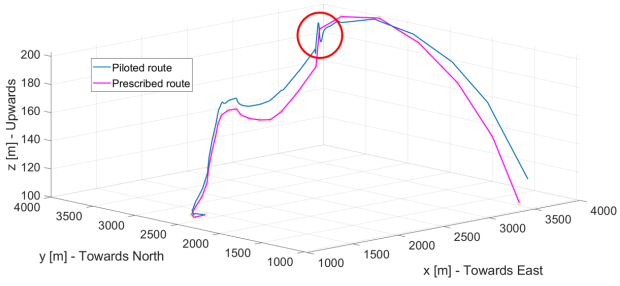

Figure 11: Prescribed vs. followed replanned route

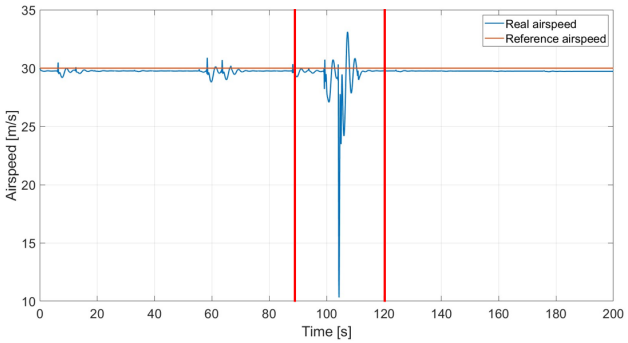

Figure 13: Airspeed vs. reference airspeed, replanned route

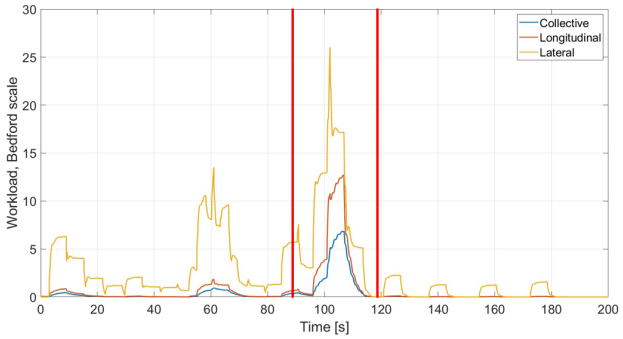

Figure 14: Workload, replanned route

4. CONCLUSION AND FUTURE WORK

A virtual-pilot-in-the-loop simulation environment has been set up in order to analyze the feasibility of the trajectories planned by a path planner based on the Rapidly-exploring Random Tree algorithm.
The helicopter has been modeled as a linear state-space dynamics, and the pilot has been modeled by means of the revised optimal control pilot model (ROCM). The pilot's neuromuscular dynamics and processing delay were modeled as second-order dynamics, augmenting the system states from 9 to 25.
A guidance logic has been implemented to allow the trajectory tracking.
The pilot's workload has been assessed by means of the computation of the aggression factor, related to the control input rates.
The pilot-in-the-loop simulator described performs a good trajectory tracking, but highlights some level of criticality connected both to endogenous and exogenous reasons:

- the simulator guidance logic generates a non-smooth and discontinuous reference, and this brings to excessive rates and control inputs which may be the cause of an apparently very high workload;
- the path planner smoothing filter fails in some portions of the trajectory to provide a smooth output. The reason has to be investigated, and the pilot-in-the-loop simulator can be a good tool to do it.

In future works, the simulator will be extended to non-linear helicopter dynamics in order to achieve a higher fidelity level of representation.

APPENDIX A: STATE-SPACE MATRICES

Here are reported the state-space A and B matrices evaluated at an airspeed of 30 m/s in straight level flight for the Lynx, Puma and Bo105 helicopters.
The velocity states u, v, w are expressed in [m/s], the attitude states in [°], the rate states in [°/s]. The control inputs are expressed in [°].

Lynx

$$\mathbf{A} = \begin{bmatrix} -0.0243 & 0.0392 & -0.6705 & -9.8014 & -0.0041 & -0.1190 & 0.0000 & 0.0000 & 0.0000 \\ -0.0467 & -0.7285 & 30.8640 & -0.4200 & -0.0186 & -0.3216 & 0.3117 & 0.0000 & 0.0000 \\ 0.0280 & 0.0248 & -2.2156 & 0.0000 & 0.0159 & 0.4108 & 0.0000 & 0.0000 & 0.0000 \\ 0.0000 & 0.0000 & 0.9995 & 0.0000 & 0.0000 & 0.0000 & 0.0000 & 0.0318 & 0.0000 \\ 0.0035 & 0.0159 & -0.1293 & 0.0133 & -0.1228 & 0.6465 & 9.7964 & -30.5334 & 0.0000 \\ -0.0437 & 0.2611 & -2.0532 & 0.0000 & -0.1713 & -10.6565 & 0.0000 & -0.2069 & 0.0000 \\ 0.0000 & 0.0000 & -0.0014 & 0.0000 & 0.0000 & 1.0000 & 0.0000 & 0.0429 & 0.0000 \\ -0.0273 & 0.0109 & -0.1661 & 0.0000 & 0.0529 & -1.8568 & 0.0000 & -0.9039 & 0.0000 \\ 0.0000 & 0.0000 & 0.0000 & 0.0000 & 0.0000 & 0.0000 & 0.0000 & 1.0000 & 0.0000 \end{bmatrix}$$

$$\mathbf{B} = \begin{bmatrix} 4.6289 & -8.0560 & 2.0386 & 0.0000 \\ -107.3896 & -21.2288 & 0.0000 & 0.0000 \\ 10.7004 & 27.6889 & -5.8115 & 0.0000 \\ 0.0000 & 0.0000 & 0.0000 & 0.0000 \\ 1.4472 & -1.6712 & -9.3018 & 3.7509 \\ 31.4636 & -27.4424 & -153.3177 & -0.7505 \\ 0.0000 & 0.0000 & 0.0000 & 0.0000 \\ 14.5826 & -5.9178 & -27.0369 & -10.1087 \\ 0.0000 & 0.0000 & 0.0000 & 0.0000 \end{bmatrix}$$

Puma

$$\mathbf{A} = \begin{bmatrix} -0.0210 & 0.0073 & 0.3765 & -9.8099 & 0.0091 & 0.3432 & 0.0000 & 0.0000 & 0.0000 \\ -0.0795 & -0.7421 & 30.8776 & -0.0907 & 0.0250 & 0.4551 & -0.2475 & 0.0000 & 0.0000 \\ 0.0066 & -0.0200 & -0.6761 & 0.0000 & -0.0062 & -0.2323 & 0.0000 & 0.0000 & 0.0000 \\ 0.0000 & 0.0000 & 0.9996 & 0.0000 & 0.0000 & 0.0000 & 0.0000 & -0.0252 & 0.0000 \\ -0.0056 & -0.0206 & 0.3314 & -0.0022 & -0.1124 & -0.4077 & 9.8067 & -30.5902 & 0.0000 \\ -0.0068 & -0.0541 & 0.7943 & 0.0000 & -0.0525 & -1.5530 & 0.0000 & 0.1467 & 0.0000 \\ 0.0000 & 0.0000 & 0.0002 & 0.0000 & 0.0000 & 1.0000 & 0.0000 & 0.0092 & 0.0000 \\ 0.0120 & 0.0242 & -0.0788 & 0.0000 & 0.0304 & -0.1347 & 0.0000 & -0.5884 & 0.0000 \\ 0.0000 & 0.0000 & 0.0000 & 0.0000 & 0.0000 & 0.0000 & 0.0000 & 1.0000 & 0.0000 \end{bmatrix}$$

$$\mathbf{B} = \begin{bmatrix} -0.7331 & -9.4443 & 0.4325 & 0.0000 \\ -98.2248 & -21.6573 & 0.0000 & 0.0000 \\ 0.6804 & 6.4103 & -0.2917 & 0.0000 \\ 0.0000 & 0.0000 & 0.0000 & 0.0000 \\ -2.2031 & -0.0321 & 9.7074 & 4.1752 \\ -5.9234 & -0.2301 & 23.2099 & 2.0758 \\ 0.0000 & 0.0000 & 0.0000 & 0.0000 \\ -7.1877 & 0.9154 & 2.6188 & -8.2872 \\ 0.0000 & 0.0000 & 0.0000 & 0.0000 \end{bmatrix}$$

Bo105

$$\mathbf{A} = \begin{bmatrix} -0.0259 & 0.0031 & 0.5799 & -9.8104 & -0.0019 & 0.0469 & 0.0000 & 0.0000 & 0.0000 \\ -0.0681 & -0.7526 & 30.8197 & -0.0352 & -0.0124 & -0.2691 & 0.2558 & 0.0000 & 0.0000 \\ 0.0331 & 0.0155 & -3.8998 & 0.0000 & 0.0118 & -0.2152 & 0.0000 & 0.0000 & 0.0000 \\ 0.0000 & 0.0000 & 0.9997 & 0.0000 & 0.0000 & 0.0000 & 0.0000 & 0.0261 & 0.0000 \\ 0.0022 & 0.0099 & 0.0520 & 0.0009 & -0.1041 & -0.6331 & 9.8070 & -30.5612 & 0.0000 \\ -0.0752 & 0.2249 & 1.1333 & 0.0000 & -0.2813 & -13.7516 & 0.0000 & 0.3075 & 0.0000 \\ 0.0000 & 0.0000 & -0.0001 & 0.0000 & 0.0000 & 1.0000 & 0.0000 & 0.0036 & 0.0000 \\ -0.0387 & -0.0035 & 0.4570 & 0.0000 & 0.1041 & -2.1940 & 0.0000 & -0.9847 & 0.0000 \\ 0.0000 & 0.0000 & 0.0000 & 0.0000 & 0.0000 & 0.0000 & 0.0000 & 1.0000 & 0.0000 \end{bmatrix}$$

$$\mathbf{B} = \begin{bmatrix} 0.3538 & -8.0368 & 3.3259 & 0.0000 \\ -108.0952 & -22.2694 & 0.0000 & 0.0000 \\ 12.2033 & 45.8401 & -17.7685 & 0.0000 \\ 0.0000 & 0.0000 & 0.0000 & 0.0000 \\ 0.3505- & 3.0808 & -8.4369 & 5.6547 \\ 16.7547 & -61.2387 & -169.9602 & 6.9482 \\ 0.0000 & 0.0000 & 0.0000 & 0.0000 \\ 13.4132 & -11.7472 & -28.9891 & -17.3339 \\ 0.0000 & 0.0000 & 0.0000 & 0.0000 \end{bmatrix}$$

APPENDIX B: LYNX AND BO105 RESULTS

Lynx Here are reported the results of the simulations for the Lynx helicopter.

Reference route

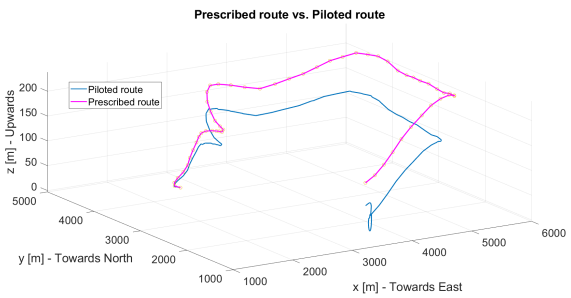

Figure 15: Prescribed vs. followed reference route, Lynx

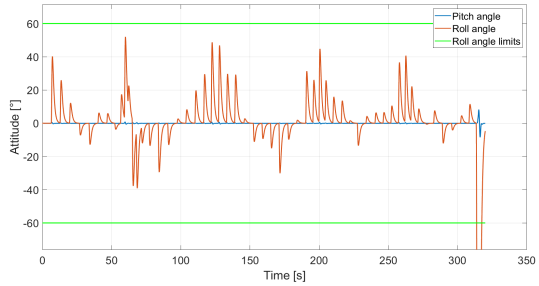

Figure 16: Attitude vs. attitude limits, reference route, Lynx

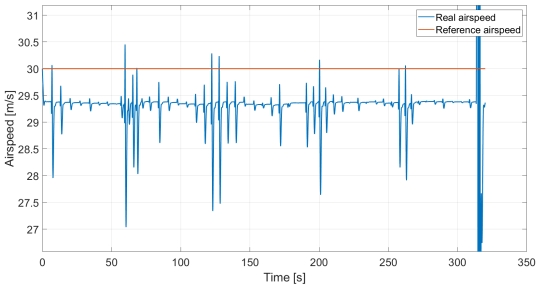

Figure 17: Airspeed vs. reference airspeed, reference route, Lynx

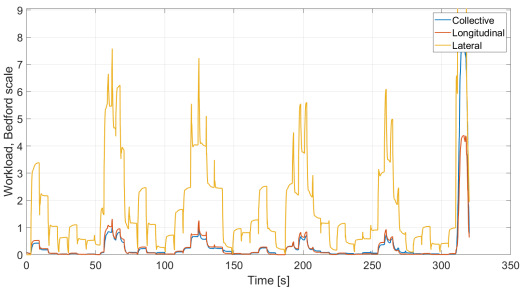

Figure 18: Workload, reference route, Lynx

Replanned route

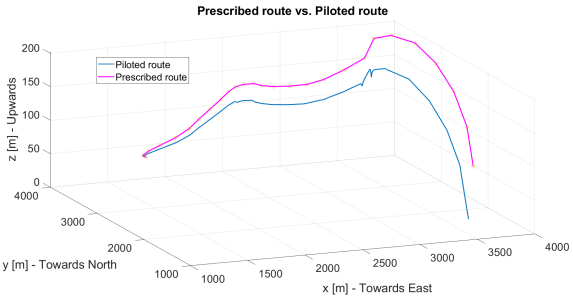

Figure 19: Prescribed vs. followed replanned route, Lynx

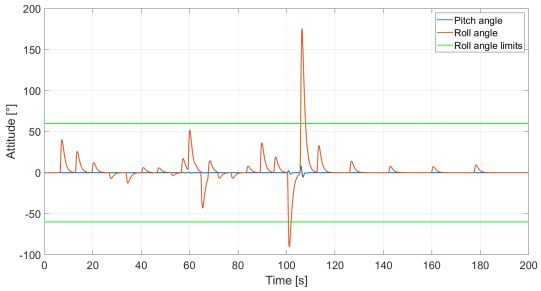

Figure 20: Attitude vs. attitude limits, replanned route, Lynx

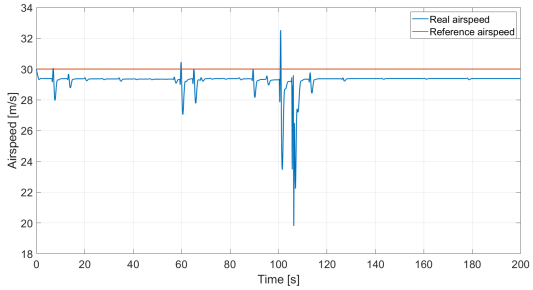

Figure 21: Airspeed vs. reference airspeed, replanned route, Lynx

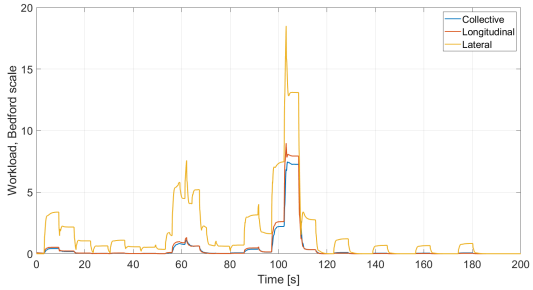

Figure 22: Workload, replanned route, Lynx

Bo105 Here are reported the results of the simulations for the Bo105 helicopter.

Reference route

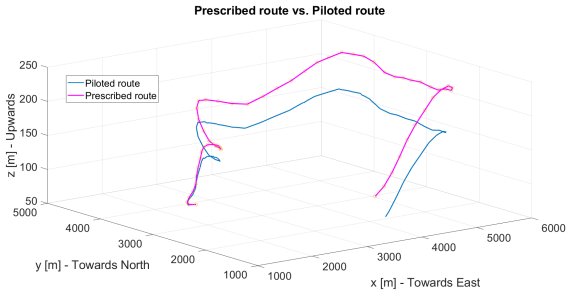

Figure 23: Prescribed vs. followed reference route, Bo105

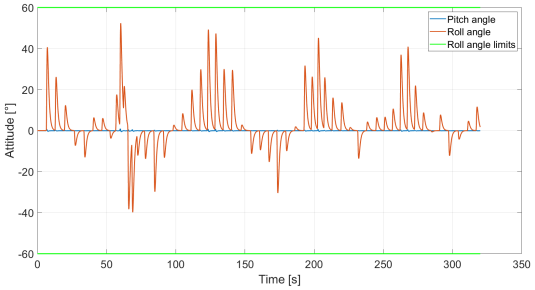

Figure 24: Attitude vs. attitude limits, reference route, Bo105

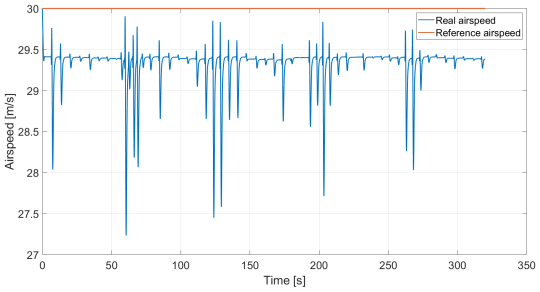

Figure 25: Airspeed vs. reference airspeed, reference route, Bo105

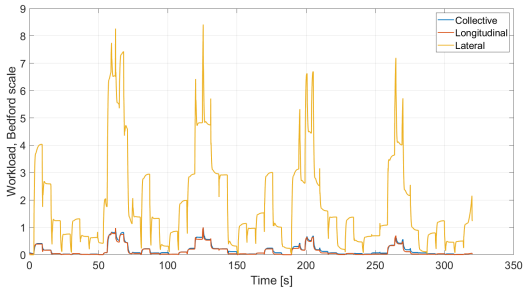

Figure 26: Workload, reference route, Bo105

Replanned route

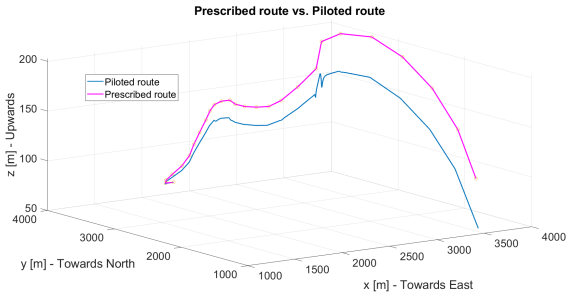

Figure 27: Prescribed vs. followed replanned route, Bo105

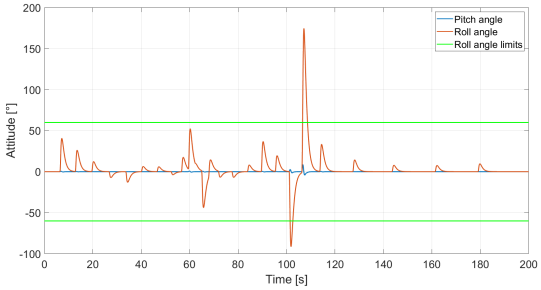

Figure 28: Attitude vs. attitude limits, replanned route, Bo105

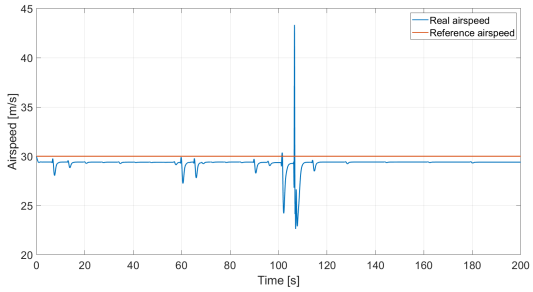

Figure 29: Airspeed vs. reference airspeed, replanned route, Bo105

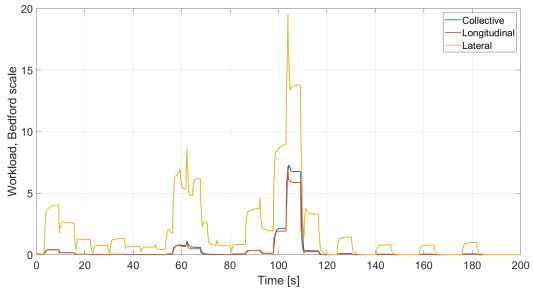

Figure 30: Workload, replanned route, Bo105

COPYRIGHT STATEMENT

References

[1] GD Padfield. Rotorcraft virtual engineering; supporting life-cycle engineering through design and development, test and certification and operations. *The Aeronautical Journal*, 122(1255):1475–1495, 2018.

[2] Giuseppe Quaranta, Stefan van't Hoff, Michael Jones, Linghai Lu, and Mark White. Challenges and opportunities offered by flight certification of rotorcraft by simulation. 2021.

[3] Arrigo Avi, Nicola Frisco, Mattia Giurato, Marco Lovera, Pierangelo Masarati, Simone Panza, Gianluca Parnesari, Francesca Roncolini, Michele Sesana, Giuseppe Quaranta, et al. Scout drone: a drone-helicopter collaboration to support hems missions. In *48th European Rotorcraft Forum (ERF 2022)*, pages 1–8, 2022.

[4] Francesca Roncolini, Giovanni Galante, Giuseppe Quaranta, Pierangelo Masarati, et al. Path planning for innovative solutions based on uav-helicopter cooperation in hems missions. In *48th European Rotorcraft Forum (ERF 2022)*, pages 1–12, 2022.

[5] Gareth D Padfield. *Helicopter flight dynamics: the theory and application of flying qualities and simulation modelling*. John Wiley & Sons, 2008.

[6] Francesca Roncolini and Giuseppe Quaranta. Virtual pilot: a review of the human pilot's mathematical modeling techniques. In *10th EUCASS - 9th CEAS Aerospace Europe Conference (AEC 2023)*, pages 1–14, 2023.

[7] Ronald A Hess. Simplified approach for modelling pilot pursuit control behaviour in multi-loop flight control tasks. *Proceedings of the Institution of Mechanical Engineers, Part G: Journal of Aerospace Engineering*, 220(2):85–102, 2006.

[8] Chunguang Wang, Feng Liao, Junwei Han, and Guixian Li. A revised optimal control pilot model for computer simulation. In *2008 2nd International Conference on Bioinformatics and Biomedical Engineering*, pages 844–848. IEEE, 2008.

[9] David L Kleinman, S Baron, and WH Levison. An optimal control model of human response part i: Theory and validation. *Automatica*, 6(3):357–369, 1970.

[10] RE Magdaleno and MC RUER. Experimental validation and analytical elaboration for models of the pilot's neuromuscular subsystem in tracking tasks(experimental validation and analytical elaboration for models of pilot neuromuscular subsystem in tracking tasks). 1971.

[11] Andrea Zanoni, Pierre Garbo, and Giuseppe Quaranta. Online evaluation of helicopter pilot workload during flight simulator experiments. In *AIAA Scitech 2022 Forum*, page 0511, 2022.

[12] Timothy McLain, Randall W Beard, and Mark Owen. Implementing dubins airplane paths on fixed-wing uavs. 2014.